A Novel Pet Tracer 18f-labeled Thiamine: Synthesis, Metabolic Kinetics, and Evaluation on Cerebral Thiamine Metabolism Status

Changpeng Wang
Zhongshan Hospital Fudan University
Siwei Zhang
Jiangsu Huayi Technology Co., Ltd., Jiangsu
Yuefei Zou
Jiangsu Huayi Technology Co., Ltd., Jiangsu
Hongzhao Ma
Jiangsu Huayi Technology Co., Ltd., Jiangsu
Donglang Jiang
Huashan Hospital Fudan University
Lei Sheng
Zhongshan Hospital Fudan University
Shaoming Sang
Zhongshan Hospital Fudan University
Lirong Jin
Zhongshan Hospital Fudan University
Yihui Guan
Huashan Hospital Fudan University
Yuan Gui
Jiangsu Huayi Technology Co., Ltd., Jiangsu
Zhihong Xu
Jiangsu Huayi Technology Co., Ltd., Jiangsu
Chunjiu Zhong (zhongcj@163.com)
Zhongshan Hospital Fudan University

Original research

Keywords: Thiamine,18F-labeled thiamine, tracer,positron emission tomography

Posted Date: May 14th, 2020

DOI: https://doi.org/10.21203/rs.3.rs-28109/v1

Version of Record: A version of this preprint was published on October 20th, 2020. See the published version at https://doi.org/10.1186/s13550-020-00710-5.

Abstract

Background: Someneuropsychological diseases are associated with abnormal thiamine metabolism, including Korsakoff-Wernicke syndrome and Alzheimer's disease. However, *in vivo* detection of brain thiamine metabolism status isstill unavailable and needs to be developed.

Methods:A novel PET tracer ^{18}F-labeled thiaminewasautomatically radio-synthesized via a two-step route. The main parameters of characterization were proved by high performance liquid chromatography (HPLC). Metabolic kinetics of ^{18}F-labeled thiamine and the status of cerebral thiamine uptakein mice and marmosets were studied by micro-positron emission tomography (PET)/computer tomography imaging. Also, *in vivo* stability, renal excretion rate, biodistribution, and the correlation between cerebral ^{18}F-labeled thiamine retention and blood thiamine levels were investigated.

Results: The ^{18}F-labeled thiamine was stableboth *in vitro* and *in vivo*and manifested fast uptake and clearance *in vivo*. The biodistribution of ^{18}F-labeled thiamine were consistent with previously reports on thiamine distribution in mice. The retention of cerebral ^{18}F-labeled thiamine was higher in mice with thiamine deficiency than that in control mice, and negatively correlated with blood thiaminediphosphate levels in marmosets.

Conclusion: The ^{18}F-labeled thiamine met the requirements for ideal PET tracer to *in vivo*evaluate the status of cerebral thiamine metabolism. This study laid the foundation for further studies on the relevant diseases.

Introduction

Thiamine, also named vitamin B_1, is an essential nutrient that can only be acquired via dietary. Once absorbed from gastrointestinal tract, thiamine is delivered to all organs and tissues by circulation and phosphorylated to thiamine diphosphate (TDP) and thiamine monophosphate (TMP) [1]. Thiamine deficiency (TD) results in lactic acidosis, mitochondrial dysfunction, and energy deficits in brain, muscle, and heart, causing a broad range of clinical manifestations, such as anorexia, agitation, diminished tendon reflexes, ataxia, disturbance of consciousness, muscle pain, and heart failure, etc [2, 3]. TD is associated with Wernicke–Korsakoff syndrome, Alzheimer's disease (AD), beriberi, Leigh syndrome, and so forth [2, 4].

The organ most affected by TD is brain [5–8]. Glucose is the predominant energy source of brain for maintaining physiological activities [9], which makes the brain vulnerable to glucose dysmetabolism. TDP, as the active form of thiamine, is the common coenzyme of the three key enzymes in glucose catabolism: pyruvate dehydrogenase and α-ketoglutarate dehydrogenase in the Krebs cycle, and transketolase in pentose phosphate pathway (PPP). Krebs cycle mainly produces ATP in mitochondria, while PPP generates antioxidants and the substrate for biosynthesizing DNA, RNA, and fatty acid in cytosol [10]. Hence, TD will impair brain function by inducing brain energy failure and a cascade of

pathophysiological alterations, such as lactic acidosis, glutamate accumulation, oxidative stress, DNA damage, etc. [2, 11, 12].

However, *in vivo* detection of cerebral thiamine metabolism status is still unavailable. In this study, a novel PET radiotracer—^{18}F-labeled thiamine was designed and synthesized (was named as MVBF, see Fig. 1) and its metabolic kinetics was studied. Cerebral thiamine metabolism status was assayed in mice and marmosets using MVBF.

Materials And Methods

1. General Information

All reagents were purchased from TCI Development Co., Ltd (Shanghai). and J & K Scientific (Beijing, China) unless otherwise indicated. Thin layer chromatography (TLC) was performed with silica gel layers, and compounds were visualized under UV light. The ^{1}H NMR (300 MHz) spectra of all compounds were acquired on an Advance (Bruker) spectrometer; chemical shifts (δ) for the proton resonance were reported in parts per million (ppm) downfield from TMS ($\delta = 0$). The analysis of mass spectra under electrospray ionization and purity of precursors were determined by a LC-MS instrument (1200/6120, Agilent Technologies Inc.) with a C_{18} column (4.6 × 150 mm 5uM; VP-ODS, Shimadzu) at 0.5 ml per minute (ml/min) flow rate. The mobile phase consisted of 60% methanol and 40% H_2O containing 1‰ formic acid.

$^{18}F^-$ ions were received from a cyclotron (Cyclone 18 Twin, IBA, Belgium), situated at the Molecular Imaging institute, Jiangsu Huayi Technology Co., Ltd., by proton irradiation of ^{18}O-enriched water. For automatic synthesis of MVBF, we used a remote-controlled radiolabeling module (RNplus, Synthra) with slight modifications and created the sequence program, based on manual trials. The scheme of modified RNplus module is presented in Fig. 2. We used six reagent supply vials (A1-A5, B1) at the upper part and two reaction vials (vial I and vial II) at the bottom part.

Analytical HPLC (1260, Agilent Technologies Inc.) with the same type column mentioned above was employed for MVBF characterization and identification. The signal acquisition system consisted of a UV detector (254 nm) and a radio-detector (1IINaI/PMT, Lablogic, USA) in series. The flow rate was 0.8 ml/min and the mobile phase consisted of methanol and H_2O containing 0.05% triethylamine and 50 mM ammonium acetate. The percentage of methanol/H_2O changed with running time: 0–15 minutes (mins), 15%/85%; 15–25 min, methanol increasing to 100% while H_2O decreasing to 0%; 25–30 min, methanol 100%.

A micro-PET/CT equipment (Inveon; Siemens Co., USA) was used for the imaging of mice and marmosets, the body temperature was maintained at 37 °C using a heat pad.

2. Synthesis of Cold Standard Sample of MVBF as Well as Precursors (5) and (6).

We synthesized cold standard sample of MVBF as well as precursors (5) and (6) according to the work of Cline JK, et al.[13], with minor modifications (Supplementary Fig. 1). The purity of the standard sample is > 99.9%, and the purity of two precursors > 99%, identified via LC-MS (Supplementary Fig. 2). The details of the synthetic route were described in the Supplementary text.

3. Automated Radiosynthesis Of Mvbf

We adopted a two-step synthesis route (Fig. 1). The scheme of automated synthesis was shown in Fig. 2. Reagents were added into supply vials as follows: A1: 1.1 ml eluent (3.08 mg $KHCO_3$, 11 mg Kryptofix 2.2.2, 0.88 mL MeCN, 0.22 mL H_2O); A2: 1 ml MeCN; A3: 5 mg precursor **(6)** in 0.5 ml MeCN; A4: 1 ml MeCN; A5: 0.5 ml MeCN; B1: 0.5 ml H_2O. 5 mg precursor **(5)** powder was also added into reaction vial II beforehand. When the first step synthesis finished, the intermediate product [^{18}F]-compound **(7)** was transferred from reaction vial I to reaction vial II via distillation. The whole automated synthesis duration was 100 min. The details of synthesis and purification were described in the Supplementary text.

4. Characteration And Quality Control Of Mvbf

Radiochemical yield (RCY, decay-correction to the end of bombardment) and radiochemical concentration (RCC) were measured by the radioactivity calibrator (CRC-55tR, CAPINTEC, INC., USA). The identity of MVBF was determined by co-injecting final product with cold standard sample into analytical HPLC. Radiochemical purity (RCP) and specific radioactivity (SA) were calculated by means of the area under curve (AUC) of radio-signals and UV-signals of final product in analytical HPLC, respectively. Bacteria and endotoxin detections were carried out by means of anaerobic/aerobic bacteria media and Limulus reagent gel methods, respectively, according to Chinese Pharmacopoeia.

5. In *Vitro* Stability

MVBF solution was stored at RT and injected into analytical HPLC for evaluating RCP and peak shape at 0 hour (h), 2 h, 4 h, 6 h, 8 h, and 10 h, respectively after synthesized.

6. Thiamine Deficiency Mouse Model And Marmosets

Eight-week-old male C57BL/6 mice and Institute of Cancer Research (ICR) mice (obtained from the SLAC Laboratory Animal Company, China) were housed in a controlled environment at temperature of 20–26 ^{o}C and humidity of 40–70% with free access to food and water. The mice were randomly divided into two

groups: TD group (n = 2 for C57BL/6, one died due to anesthesia during micro-PET/CT scanning; n = 3 for ICR), which was fed thiamine-depleted diet (Trophic Animal Feed High-tech Co., Ltd., China), and control group (n = 3 for each strain), which was fed general diet. Twenty-eight days later, all mice received PET/CT scanning.

Four marmosets aged 3.1–10.8 years old (supplied by Jiuting Non-human Primate Facility, Chinese Academy of Sciences, Shanghai) were employed for micro-PET/CT scanning. At the day of experiment, the marmosets were fetched from the facility.

After scanning, the mice were sacrificed and the marmosets were sent back to the facility. The blood of the animals was collected for measuring thiamine levels.

7. Dynamical Micro-PET/CT Images and Evaluation of Cerebral Thiamine Metabolism Status

Micro-PET/CT imaging using MVBF as a tracer for evaluating cerebral thiamine metabolism status was performed in TD mice model and control mice, as well as in marmosets. The animals were anesthetized by inhalation of 1.5%-2% isoflurane in air (1.5 L/min) and received CT scan for acquiring structure image and attenuation correction data. Then, the mice were injected with 7.4–14.8 MBq MVBF in 0.1 ml volume (diluted by normal saline) through the tail vein and immediately scanned dynamically for 90 min with an energy window of 350-650KeV and a time window of 3.438 ns. A total of 35 frames were setup: 20f, 3 s; 4f, 60 s; 5f, 300 s; 6f, 600 s. Dynamic images were reconstructed by OSEM3D/SP-MAP algorithm with two iterations. The marmosets were injected with 46.3–74.0 MBq MVBF in 0.5–0.8 ml volume through the femoral vein and immediately scanned dynamically for 60 min. A total of 18 frames was setup: 6f, 10 s; 4f, 60 s; 5f, 300 s; 6f, 600 s. The other conditions for marmosets were the same as for mice.

Regions of interest (ROIs) were drawn manually over the whole brain (for mice and marmosets) and in the left ventricular cavity (for marmosets) based on the PET/CT co-registered images using IRW 4.2 software (Siemens Medical Solutions USA, Inc.). Radioactivity was expressed as standard uptake value (SUV): (ROI radioactivity/ROI volume)/(injected radioactivity/gram of body weight). The time-activity curve (TAC) and AUC (SUV*mins) were also calculated.

The TACs of the marmosets blood (Radioactivity was expressed as SUV) were taken as input functions (IF) [14–16] for fitting Patlak plots [17, 18], in order to analyze transfer constants (K_i) of brains in marmosets (IRW 4.2 software). The details of Patlak model was described in the supplemental text.

8. Measurement of Thiamine, TMP, and TDP in Whole Blood Samples of Mice and Marmosets

Thiamine, TMP, and TDP levels in whole blood samples were measured using HPLC, based on the established mothed [4] with slight modification. Briefly, blood samples were collected using heparin-anticoagulated tubes, 150 ul sample was vibrated for 30 s with equal volume 5.7% (for mice) or 5.2% (for marmosets) perchloric acid (PCA) added dropwise for deproteinization. Then, the mixture was stored at -80^{o}C until assay within one month. The mixture was centrifuged at 12000 rpm for 8 min at 4 ^{o}C, the supernatant was pipetted. Thiamine, TMP, and TDP in supernatant were derivatized into thiochromes using potassium ferricyanide and analyzed by gradient elusion with C_{18} reversed-phase analytical column (250 × 4.6 mm). The derivatives were identified by HPLC fluoroscopy (1100, Agilent Technologies Inc., ex: 367 nm, em: 435 nm). The thiamine, TMP, and TDP levels were quantified using standard samples (Sigma-Aldrich, St. Louis, MO). The analyzers were blinded to samples information.

9. Pharmacokinetic and Metabolic Kinetics Studies in Liver and Kidney of Mice

Nine-week-old male ICR mice (n = 5, SLAC Laboratory Animal Company) were dynamically scanned using micro-PET/CT for 60 min. A total of 18 frames was reconstructed: 6f, 10 s; 4f, 60 s; 5f, 300 s; 6f, 600 s. The housing environment and the other scanning conditions were the same as mentioned above. ROIs of the liver and renal parenchyma as well as the left ventricular cavity were manually drawn.

For Pharmacokinetic Study, the TACs of the blood were fitted. The radioactivity was evaluated as %ID/g (the percentage of injected dose per gram of blood). Pharmacokinetics parameters were counted through the software PKSolver (version 2.0, China Pharmaceutical University) [19].

For metabolic kinetics study, SUV, TAC, AUC, maximum radioactivity (C_{max}), and time to C_{max} (T_{max}) were calculated. The TACs of the blood (Radioactivity expressed as SUV) were taken as IFs for fitting Logan plots [20, 21], in order to analyze the distribution volumes (V_D) of MVBF in liver and kidney, respectively (IRW 4.2 software). The details of Logan model were described in the supplemental text.

10. Biodistribution Study

The biodistribution of MVBF was studied on ICR mice (n = 36 in total; 18 males, nine-weeks-old, 33.5 ± 4.0 g; 18 females, seven-week-old, 27.7 ± 5.0 g). MVBF solution was diluted to 37 MBq/ml, and for each mouse, 0.1 ml MVBF was injected into the tail vein under isoflurane anesthesia. The mice were sacrificed at 2 min, 10 min, 30 min, 1 h, 2 h, and 4 h after administration (3 males and 3 females for each time point). The tissues of heart, liver, spleen, lung, kidney, stomach, duodenum, pancreas, femur, muscle (from thigh), blood, brain, fat, and gonad (ovary or testicle) were harvested, weighted, and measured for radioactivity by γ-counter. %ID/g was calculated referring to the counts of standard samples.

11. *In Vivo* Stability and the Renal Excretion Rate

After metabolic kinetics study and waking from anesthesia, the urine samples from three ICR mice were collected and measured in the radioactivity calibrator. The duration from MVBF injection to urine collection was about 85 min. Then, 0.1 ml urine for each mouse was added in an Eppendorf tube, vibrated for 30 s with equal volume PCA added dropwise for deproteinization. After centrifuging at 12000 rpm for 8 min at 4 ^{o}C, the supernatant was filtered and analyzed using HPLC.

12. Statistical Analysis

For the continuous data, mean ± SEM was applied for statistical description. Student *t* test was employed to compare the AUC values between TD mice and controls in ICR strain. The Pearson correlation was utilized to analyse the correlation between the cerebral accumulation of MVBF and the blood levels of thiamine, TMP, and TDP in marmosets. Repeated measurement of ANOVA with Trukey's *post-hoc* was used to analyse the AUC values of MVBF between brain, liver, and kidney in ICR mice. All statistical analyses were performed using SPSS (Statistical Package for the Social Sciences) software (version 22.0; SPSS Inc., Chicago IL).

Results

1. Characteration and Quality Control of MVBF

The identity, RCP, and SA of MVBF were confirmed (Fig. 3). All relevant items of characterization were shown in Table 1. The solution was clean. The RCP and SA were > 97% and > 55.5 GBq/umol, respectively. The RCY was 7%-11% (decay-corrected to the end of bombardment), and the RCC was 740–1110 MBq/ml. The bacteria and endotoxin tests were negative. In addition, MVBF final product was stable at RT, with the RCP > 95% six hours, and > 93% ten hours after synthesis (Table 2).

Table 1
Characteration and Quality Control of MVBF

Items	Results
Physical character	clear and transparent, no macroscopic impurity
Ph value	4.5
Alcohols	0%
RCP	> 97%
SA	> 55.5 GBq/umol
RCY (n = 3)[a]	7%-11%
RCC (n = 3)	740–1110 MBq/ml
bacteria test	negative
endotoxin test	negative
a. decay-corrected to the end of bombardment.	

Table 2
In Vitro Stability Test of MVBF

Time after synthesis (hours)	RCP
0	> 97%
2	> 96%
4	> 96%
6	> 95%
8	> 94%
10	> 93%

2. Evaluation Of Cerebral Thiamine Metabolism Status

For C57BL/6 mice, the cerebral retention of MVBF had been increasing within 90 min, and approached to C_{max} at the terminal time in the two mice with TD. The $SUVs_{max}$ of the last frame (80–90 min) were 0.48 (TD 3) and 0.55 (TD 5), and the AUC values within 90 min were 34.99 (TD 3) and 42.46 (TD 5). In contrast, the cerebral retention was stable within 90 min in the three control mice, the $SUVs_{max}$ were about 0.17 (Ctrl 2), 0.25 (Ctrl 4), and 0.3 (Ctrl 1). The AUC values within 90 min were 14.52 (Ctrl 2), 20.96 (Ctrl 4), and 25.67 (Ctrl 1) (Fig. 4A-B). The mean AUC value in TD mice was 1.9 times higher than that in control mice (38.73 ± 3.74 vs. 20.38 ± 3.23).

For ICR mice with TD, the cerebral $SUVs_{max}$ were 0.98 at 28th frame (TD 3, 20–25 min) and 0.97 at 30th frame (TD 4, 30–40 min) in two mice, then the SUVs decreased slowly. In the third mouse (TD 1), the cerebral retention of MVBF increased till the 33th frame (60–70 min), and the SUV_{max} was 0.61. The AUC values within 90 min were 79.28 (TD 3), 78.75 (TD 4), and 46.81 (TD 1), respectively. Similar to C57BL/6 mice, the SUVs were stable within 90 min in ICR control mice, about 0.36 (Ctrl 1), 0.27 (Ctrl 5) and 0.18 (Ctrl 3), respectively. The AUC values within 90 min were 29.58 (Ctrl 1), 21.14 (Ctrl 5) and 14.92 (Ctrl 3), respectively (Fig. 4C-D). The AUC values in TD mice were significantly higher than those in controls (68.28 ± 10.74 vs. 21.88 ± 4.25, P = 0.016).

The cerebral retention of MVBF had been increasing in three marmosets within 60 min (M1, M3, M4), and reached plateau at 16th frame (30–40 min) in M2. The SUV_{max} were between 0.33 to 0.90, and the AUC values within 60 min between 17.07 to 42.28 (Fig. 4E-F). Notably, a significantly negative correlation was found between cerebral AUC values within 60 min and TDP levels in whole blood samples (r = -0.985, p = 0.015, Fig. 4I), whereas no significant correlation existed between cerebral AUC values of MVBF and blood thiamine and TMP levels (Fig. 4G-H). In order to quantitatively evaluate the cerebral uptake of MVBF in marmosets, we employed Patlak model to analyze the blood-to-brain transfer rate constant K_i based on the characteristics of metabolic kinetics in brain. The regression plots were fitted automatically by software from 20 min to 60 min. K_i was between 0.0030–0.0102 ml/g/min, and significantly correlated with age (Fig. 4J, see the fitted Patlak plots in Supplementary Fig. 3).

3. Pharmacokinetic Study and Metabolic Kinetics study in liver and kidney of Mice

Table 3 showed the pharmacokinetic parameters. Figure 5A showed the TAC of MVBF (radioactivity as ID%/g) within 60 min in the blood of ICR mice. The pharmacokinetic profiles of MVBF fitted a two-compartment open model. The value of $AUC_{0-60\ min}$ was 37.313, accounting for 99.77% of the value of AUC_{0-inf} (37.399), which implies that the 60 min observation be sufficient to depict the pharmacokinetic characters. The T_{max} and the C_{max} were the first frame (0–10 sec) and 18.12 ± 2.20 ID%/g, respectively. The half-life of distribution ($t_{1/2\alpha}$) and half-life of elimination ($t_{1/2\beta}$) were 0.082 and 6.379 min, respectively. The volume of distribution (V_D1) and clearance rate (CL1) of central compartment were 3.058 g and 2.674 g/min, respectively. The V_D2 and CL2 of peripheral compartment were 19.308 g and 20.162 g/min, respectively. These results revealed that MVBF could be absorbed and eliminated rapidly.

Table 3
Pharmacokinetic Parameters of MVBF in ICR Mice (n = 5).

Parameters (Units)	Values
T_{max} (s)	0–10
C_{max} (ID%/g)	18.12 ± 2.20[a]
V_D1 (g)	3.058
CL1 (g/min)	2.674
V_D2 (g)	19.308
CL2 (g/min)	20.162
$t_{1/2}(\alpha)$ (min)	0.082
$t_{1/2}(\beta)$ (min)	6.379
$AUC_{0-60min}$ (%ID/g*min)	37.313
AUC_{0-inf} (%ID/g*min)	37.399
k_{10} (min^{-1})[b]	0.874
k_{12}(min^{-1})[b]	6.593
k_{21}(min^{-1})[b]	1.044
a. Data were expressed as mean ± SEM.	
b. K_{10}, elimination rate constant; K_{12}, elimination rate constant from central compartment to peripheral compartment; K_{21}, elimination rate constant from peripheral compartment to central compartment.	

The representative results of micro-PET/CT dynamic whole-body scanning of ICR mice within 60 min were shown as Fig. 6. Initially, MVBF distributed mainly into liver, intestine, and bladder. Then, the radioactivities in intestine and bladder were increasing while in liver fading out with time. These results demonstrated that the uptake and elimination of MVBF *in vivo* were fast, and the main accumulation and elimination organs were liver and kidney.

The T_{max} and SUV_{max} of the liver were the 6th frame (50–60 sec) and 4.61 ± 0.53, respectively. Then the SUV dropped fast to 3.23 ± 0.50 at the 10th frame (4–5 min). The radioactivity continued to decrease afterwards, and the decrease rate become smaller and smaller within 60 min. The SUV was 0.72 ± 0.05 at the terminal time. The AUC value within 60 min was 79.94 ± 5.43 (Fig. 5B). The T_{max} and SUV_{max} of the kidney were the 4th frame (30–40 sec) and 18.67 ± 7.04, respectively. The SUV dropped fast to 3.29 ±

0.50 at the 11th frame (5–10 min), and continued to drop slowly. At the terminal time, the SUV dropped to 0.77 ± 0.35. The AUC value was 113.4 ± 15.56 (Fig. 5C). The AUC values of liver and kidney within 60 min were significantly higher than that of whole brain ($P < 0.001$). Also, the value of kidney was significantly higher than that of liver ($P < 0.05$, Fig. 5D).

Logan plot was applied to analyze the distribution volume V_D of liver and kidney based on the characteristics of metabolic kinetics in these two organs. The regression plots were fitted automatically by software from 10 min to 60 min, and V_D were 4.573 ± 0.34 ml/g for liver and 6.17 ± 0.88 ml/g for kidney (Supplementary Fig. 4A-E, 5A-E). The results indicated that the “steady-state” of uptake/clearance of these two organs was achieved since the 10th min, the mean uptake amount of MVBF per gram tissue was equivalent to the amount contained in 4.573 ml (for liver) or 6.17 ml (for kidney) blood.

4. *In Vivo* Stability and Renal Excretion Rate

Since the -OH group of thiamine is replaced by -^{18}F, MVBF cannot enter the known metabolic pathways of thiamine before ^{18}F decays back to ^{18}O [22, 23]. We collected about 0.1 ml urine per ICR mouse in total within 85 min after tail vain injection. The radioactivity in urine was 34.16 ± 3.84% of total injected radioactivity measured by radioactivity calibrator (decay-correction), and no correlation was found between the excreted radioactivity in urine and the injected radioactivity (Supplementary Table 1). The RCP of renal excreted MVBF was 94.53 ± 0.81% determined by HPLC, and an unknown trace metabolite (3.30 ± 0.60% in RCP) existed ahead of MVBF and could not be detached $^{18}F^-$ ions according to its retention time and shape (Fig. 7). These results indicated that through 85 min of *in vivo* metabolism, 1) about one third MVBF was excreted by kidney, 2) MVBF was virtually stable, 96.63% in urine was prototype, 3) about 3.37% MVBF was metabolized to more polar unknown compounds.

5. Biodistribution Study

As a derivative of an essential vitamin, MVBF distributed widely *in vivo*. In most of the organs and tissues of male ICR mice, the C_{max} of MVBF achieved between 5 to 15 min, then MVBF was cleared rapid and the accumulation was very low in these organs and tissues till 4 hours after injection. The accumulation of MVBF in muscle was increasing within 60 min, then declining rapid, too. We found a decreasing tendency of radioactivity in bone with time, which indicated no defluorination effect of MVBF existed *in vivo* (Fig. 8A-C, Supplementary Table 2). The biodistributions in female were similar to those in male, except that the radioactivity began to decline 5 min after injection in female muscle. Also, a decreasing tendency of radioactivity in bone was found. (Fig. 8D-E, Supplementary Table 3).

Consistent with the results of PET/CT scanning, liver and kidney were the main distribution organs. Also, MVBF accumulated highly in duodenum, which indicated liver as one of the main clearance organs. The

biodistribution of MVBF in brain, fat, and gonad was less than other organs or tissues, while the ovary took in more MVBF than testicle did.

Discussion

The cerebral levels of thiamine and its phosphate esters decline progressively in mice with TD [24]. In this study, compared with control mice, the cerebral accumulation of MVBF was higher in two strains mice with TD (Fig. 4A-D). These results indicated MVBF accumulation would increase when thiamine was deficient in the brain. TDP accounts for 90% of total thiamine in the body [25]. We observed that the cerebral accumulation of MVBF significantly negatively correlated with blood TDP levels in marmosets (Fig. 4I). Besides, our laboratory found TDP levels in blood decreased with aging in marmosets (unpublished data). Here, the blood-to-brain transfer rate K_i was significantly positively correlated with aging (Fig. 4J). Together, these results from marmosets meant that the less thiamine levels in the body, the more cumulation of MVBF in the brain. Hence, MVBF could evaluate cerebral thiamine metabolism status *in vivo*.

Cerebral glucose metabolism is extremely high [26]. It leads to the possibility that mild alteration of brain glucose metabolism under pathological or physiological conditions is difficult to be detected by PET with [^{18}F]-fluorodeoxyglucose (FDG-PET). The extent of cerebral TD was consistent with that of cerebral glucose hypometabolism in rodents, and the level of blood TDP was positively correlated with that of cerebral glucose metabolism in patients with AD [24]. In this study, the cerebral SUVs of MVBF in control mice and marmosets were less than 0.4 and 0.9, respectively (Fig. 4A and C), much lower than that of FDG in mice which was in the range of 1 to 2 [27]. The phenomenon that the abundance of thiamine metabolism was much lower than that of glucose metabolism in brain implies MVBF may be more sensitive than FDG for evaluation of mild alteration in brain glucose metabolism status. The further investigations are under way.

In both genders of ICR mice, kidney, liver, duodenum, and pancreas were high accumulation tissues for MVBF, while brain, muscle, fat, and gonad were low accumulation tissues (Fig. 8; Supplementary Table 2, 3). These results are consistent with previously reports on the biodistributions of thiamine and its phosphate esters [28–30]. Besides, we found that 3.37% of MVBF in urine was metabolized to more polar compounds after 85 min *in vivo* process (Fig. 7). To our knowledge, the –OH group is the active site for thiamine metabolism *in vivo* [22, 23]. Thus, before – ^{18}F decays back to stable isotope – ^{18}O, MVBF could not enter the known metabolic routes. The presence of this 3.37% compounds implied other unknown metabolic routes might exist. MVBF could help for further exploration on the metabolism and biodistribution of thiamine.

Stability is important for PET tracer. MVBF was stable at RT. The RCP was > 95% 6 h, and > 93% 10 h after synthesis, which means no significant radiolysis effect exists *in vitro* (Table 2) [31]. In addition, no ^{18}F-deflourination of MVBF *in vivo* was observed based on the phenomenon that the accumulation of radioactivity signal in bone was decreasing over time [32] (Fig. 8B and E). Also, the prototype form of

MVBF excreted in urine reached 96.63% within 85 min after vein administration (Fig. 7). These results demonstrated MVBF was highly stable both *in vitro* and *in vivo*.

Pharmacokinetic and metabolic kinetics studies as well as biodistribution study indicated that the uptake and clearance of MVBF *in vivo* were fast, which is another important requirement. The $t_{1/2\beta}$ was 6.379 min, CL_1 and CL_2 were 2.674 g/min and 20.162 g/min, respectively (Table 3). The C_{max} in various tissues and organs of ICR mice achieved within 15 min (except for muscle of males, achieved at 1 h), and the accumulation of MVBF was very low in these tissues and organs till 4 hours after administration (Fig. 8, Supplementary Tables 2 and 3). Besides, about one third MVBF was excreted through kidney 85 min after administration (Supplementary Table 1).

Graphical analysis technique has been extensively applied in the analyses of nuclear medicine imaging data. It is especially suitable for pharmacokinetic studies of novel tracers before the compartmental models are fully described, because it is independent of any specific model configuration [21]. We analyzed the important kinetic parameters K_i and V_D in brain of marmosets and in liver and kidney of ICR mice employing Patlak and Logan plots, respectively, based on the characteristics of TACs in these organs (Fig. 4E, Fig. 5B, C). The V_D of the kidney and liver were 6.17 ± 0.88 ml/g and 4.573 ± 0.34 ml/g, respectively, which corroborated the conclusion that the uptake and clearance of MVBF *in vivo* were fast.

Thiamine consists of a pyrimidine ring with an electronegative amidogen and a thiazole ring. The structural complexity determines the difficulty of artificially synthesizing and modifying thiamine. Since the first synthesis route was reported in 1937 [13], only a few studies on thiamine synthesis and modification have been published [33–35]. Recently, Doi H, et al. synthesized radio-labelled thiamine with ^{11}C [35], and conducted heart imaging study in rats [36]. Although ^{11}C-thiamine possesses the same molecular structure as thiamine itself, the short half-life of ^{11}C (20.4 min) limits its application. Also, ^{11}C-thiamine would be phosphorylated to ^{11}C-TDP fast via the -OH group *in vivo* [36], which complicates the interpretation of the radio-signal. Via employing a two-step route, we synthesized MVBF successfully, with -OH group of thiamine replaced by -^{18}F (Fig. 1). Although the RCY was not high enough, the RCP, SA and RCC were high (Table 1). The bacteria and endotoxin tests were negative. These characterization results indicated that MVBF was safe and suitable for *in vivo* studies.

The most difficult part in our two-step route is the isolation and purification of the intermediate product ^{18}F-compound **(7)**. Though we tried various solid phase extractions as well as prep-HPLC, either the isolation failed or the process became too complicated to achieve automation. 4-methyl-5(beta-hydroxyethyl)-thiazole is solid, and its boiling point is 135^oC under vacuum [37]. Once -OH is changed to -F, however, this compound becomes oil and volatile at RT. We speculated that it was because the H bond connecting H and N was broken (Supplementary Fig. 6). Via distillation, we successfully isolated compound **(7)** and automated the radiosynthesis route.

Conclusion

In this study, we synthesized a novel PET tracer MVBF and established its automated synthesis solution. MVBF was stable *in vitro* and *in vivo*, and possessed ideal characteristics of metabolic kinetics. It could evaluate the status of cerebral thiamine metabolism, and might be more suitable for evaluating cerebral energy metabolism than FDG, due to the low abundance of cerebral thiamine metabolism. However, the sample size of marmosets in this study was not large enough, and we lack of TD model of marmosets to further investigate thiamine metabolism in non-human primates. This study laid the foundation for further studies on diseases related to thiamine dysmetabolism.

Declarations

Ethical approval

All animal care and experimental procedures were carried out according to the guidelines of the Animal Care Committee of Fudan University. This study was approved by Medical Experimental Animal Administrative Committee of Fudan University, and the committee on medical ethics of Zhongshan Hospital, Fudan University.

Consent for publication

Not applicable.

Availability of data and materials

The datasets used in the current study are available from the corresponding author onreasonable request.

Conflict of interest

Chunjiu Zhong holds shares of Shanghai Rixin Biotech Co., Ltd., which focuses on the development of new drugs against Alzheimer's disease. The other authors declare that he/she has no conflict of interest.

Funding

This study was financially supported bythe National Key Research and Development Program Foundation of China (2016YFC1306403) to Chunjiu Zhong, the National Natural Science Foundation of China (grant no. 91332201) to Chunjiu Zhong,and Zhongshan Hospital Science Foundation (2018ZSQN28) to Changpeng Wang.

Authors' contributions

Zhong C conceived the study. Zhong C and Wang C designed the study. Wang C, Zhang S, Zhou Y, Ma H, Gui Y and Xu Z were responsible for radiosynthesis. Wang C, Jiang D, Sheng L, Sang S, Jin L, and Guan Y wasresponsible for animal studies. The manuscript was drafted by Wang Cand Zhong C. All authors read and approved the final manuscript.

Acknowledgements

We thank Profess Fengling Qing, Profess Xiuhua Xu, and Doctor Zenghao Chen for their assistance in synthesis routes.

References

1. Talwar D, Davidson H, Cooney J, St JD. Vitamin B(1) status assessed by direct measurement of thiamin pyrophosphate in erythrocytes or whole blood by HPLC: comparison with erythrocyte transketolase activation assay. Clin Chem. 2000;46:704–10.
2. Dhir S, Tarasenko M, Napoli E, Giulivi C. Neurological, Psychiatric, and Biochemical Aspects of Thiamine Deficiency in Children and Adults. Front Psychiatry. 2019;10:207.
3. Hiffler L, Rakotoambinina B, Lafferty N, Martinez GD. Thiamine Deficiency in Tropical Pediatrics: New Insights into a Neglected but Vital Metabolic Challenge. Front Nutr. 2016;3:16.
4. Pan X, Fei G, Lu J, Jin L, Pan S, Chen Z, et al. Measurement of Blood Thiamine Metabolites for Alzheimer's Disease Diagnosis. EBioMedicine. 2016;3:155–62.
5. Martin PR, Singleton CK, Hiller-Sturmhofel S. The role of thiamine deficiency in alcoholic brain disease. Alcohol Res Health. 2003;27:134–42.
6. Kril JJ, Harper CG. Neuroanatomy and neuropathology associated with Korsakoff's syndrome. Neuropsychol Rev. 2012;22:72–80.
7. Opdenakker G, Gelin G, De Surgeloose D, Palmers Y. Wernicke encephalopathy: MR findings in two patients. Eur Radiol. 1999;9:1620–4.
8. Kornreich L, Bron-Harlev E, Hoffmann C, Schwarz M, Konen O, Schoenfeld T, et al. Thiamine deficiency in infants: MR findings in the brain. AJNR Am J Neuroradiol. 2005;26:1668–74.
9. Bouzier-Sore AK, Voisin P, Bouchaud V, Bezancon E, Franconi JM, Pellerin L. Competition between glucose and lactate as oxidative energy substrates in both neurons and astrocytes: a comparative NMR study. Eur J Neurosci. 2006;24:1687–94.
10. Butterworth RF, Kril JJ, Harper CG. Thiamine-dependent enzyme changes in the brains of alcoholics: relationship to the Wernicke-Korsakoff syndrome. Alcohol Clin Exp Res. 1993;17:1084–8.
11. Jankowska-Kulawy A, Bielarczyk H, Pawelczyk T, Wroblewska M, Szutowicz A. Acetyl-CoA deficit in brain mitochondria in experimental thiamine deficiency encephalopathy. Neurochem Int. 2010;57:851–6.

12. Gibson GE, Blass JP, Beal MF, Bunik V. The alpha-ketoglutarate-dehydrogenase complex: a mediator between mitochondria and oxidative stress in neurodegeneration. Mol Neurobiol. 2005;31:43–63.
13. Cline JK, Williams RR, Finkelstein J. Studies of Crystalline Vitamin B1. XVII. Synthesis of Vitamin B1. J Am Chem Soc. 1937;59:1052–4.
14. Laforest R, Sharp TL, Engelbach JA, Fettig NM, Herrero P, Kim J, et al. Measurement of input functions in rodents: challenges and solutions. Nucl Med Biol. 2005;32:679–85.
15. Lee YJ, Maeda J, Kusuhara H, Okauchi T, Inaji M, Nagai Y, et al. In vivo evaluation of P-glycoprotein function at the blood-brain barrier in nonhuman primates using [11C]verapamil. J Pharmacol Exp Ther. 2006;316:647–53.
16. Wanek T, Traxl A, Bankstahl JP, Bankstahl M, Sauberer M, Langer O, et al. [(18)F]FDG is not transported by P-glycoprotein and breast cancer resistance protein at the rodent blood-brain barrier. Nucl Med Biol. 2015;42:585–9.
17. Patlak CS, Blasberg RG, Fenstermacher JD. Graphical evaluation of blood-to-brain transfer constants from multiple-time uptake data. J Cereb Blood Flow Metab. 1983;3:1–7.
18. Patlak CS, Blasberg RG. Graphical evaluation of blood-to-brain transfer constants from multiple-time uptake data. Generalizations J Cereb Blood Flow Metab. 1985;5:584–90.
19. Zhang Y, Huo M, Zhou J, Xie S. PKSolver. An add-in program for pharmacokinetic and pharmacodynamic data analysis in Microsoft Excel. Comput Methods Programs Biomed. 2010;99:306–14.
20. Logan J, Fowler JS, Volkow ND, Wolf AP, Dewey SL, Schlyer DJ, et al. Graphical analysis of reversible radioligand binding from time-activity measurements applied to [N-11C-methyl]-(-)-cocaine PET studies in human subjects. J Cereb Blood Flow Metab. 1990;10:740–7.
21. Logan J. A review of graphical methods for tracer studies and strategies to reduce bias. Nucl Med Biol. 2003;30:833–44.
22. Bettendorff L, Wins P. Thiamin diphosphate in biological chemistry: new aspects of thiamin metabolism, especially triphosphate derivatives acting other than as cofactors. FEBS J. 2009;276:2917–25.
23. Manzetti S, Zhang J, van der Spoel D. Thiamin function, metabolism, uptake, and transport. Biochemistry. 2014;53:821–35.
24. Sang S, Pan X, Chen Z, Zeng F, Pan S, Liu H, et al. Thiamine diphosphate reduction strongly correlates with brain glucose hypometabolism in Alzheimer's disease, whereas amyloid deposition does not. Alzheimers Res Ther. 2018;10:26.
25. Lu J, Frank EL. Rapid HPLC measurement of thiamine and its phosphate esters in whole blood. Clin Chem. 2008;54:901–6.
26. de Castro IP, Martins LM, Tufi R. Mitochondrial quality control and neurological disease: an emerging connection. Expert Rev Mol Med. 2010;12:e12.

27. Wong KP, Sha W, Zhang X, Huang SC. Effects of administration route, dietary condition, and blood glucose level on kinetics and uptake of 18F-FDG in mice. J Nucl Med. 2011;52:800–7.
28. Klooster A, Larkin JR, Wiersema-Buist J, Gans RO, Thornalley PJ, Navis G, et al. Are brain and heart tissue prone to the development of thiamine deficiency? Alcohol. 2013;47:215–21.
29. Gangolf M, Czerniecki J, Radermecker M, Detry O, Nisolle M, Jouan C, et al. Thiamine status in humans and content of phosphorylated thiamine derivatives in biopsies and cultured cells. PLoS One. 2010;5:e13616.
30. Hilbig R, Rahmann H. Comparative autoradiographic investigations on the tissue distribution of benfotiamine versus thiamine in mice. Arzneimittelforschung. 1998;48:461–8.
31. Jacobson MS, Dankwart HR, Mahoney DW. Radiolysis of 2-[18F]fluoro-2-deoxy-D-glucose ([18F]FDG) and the role of ethanol and radioactive concentration. Appl Radiat Isot. 2009;67:990–5.
32. Chien DT, Szardenings AK, Bahri S, Walsh JC, Mu F, Xia C, et al. Early clinical PET imaging results with the novel PHF-tau radioligand [F18]-T808. J Alzheimers Dis. 2014;38:171–84.
33. Archer S, Perianayagam C. An attempt to apply lethal synthesis to the design of chemotherapeutic agents. Fluorinated 5 beta-(hydroxyethyl)-4-methylthiazoles. J Med Chem. 1979;22:306–9.
34. Lowe G, Potter BVL. Bacteriostatic activity of fluoro-analogues of 5-(2-hydroxyethyl)-4-methylthiazole, a metabolic intermediate in the biosynthesis of thiamine. J. Chem. Soc., Perkin Trans. 1. 1980;2026–2028.
35. Doi H, Mawatari A, Kanazawa M, Nozaki S, Nomura Y, Kitayoshi T, et al. Synthesis of (11)C-Labeled Thiamine and Fursultiamine for in Vivo Molecular Imaging of Vitamin B1 and Its Prodrug Using Positron Emission Tomography. J Org Chem. 2015;80:6250–8.
36. Nozaki S, Mawatari A, Nakatani Y, Hayashinaka E, Wada Y, Nomura Y, et al. PET Imaging Analysis of Vitamin B1 Kinetics with [(11)C]Thiamine and its Derivative [(11)C]Thiamine Tetrahydrofurfuryl Disulfide in Rats. Mol Imaging Biol. 2018;20:1001–7.
37. Amos WJ, Neal RA. Isolation and identification of 3-(2'-methyl-4'-amino-5'-pyrimidylmethyl)-4-methylthiazole-5-acetic acid (thiamine acetic acid) and 2-methyl-4-amino-5-formylaminomethylpyrimidine as metabolites of thiamine in the rat. J Biol Chem. 1970;245:5643–8.

Figures

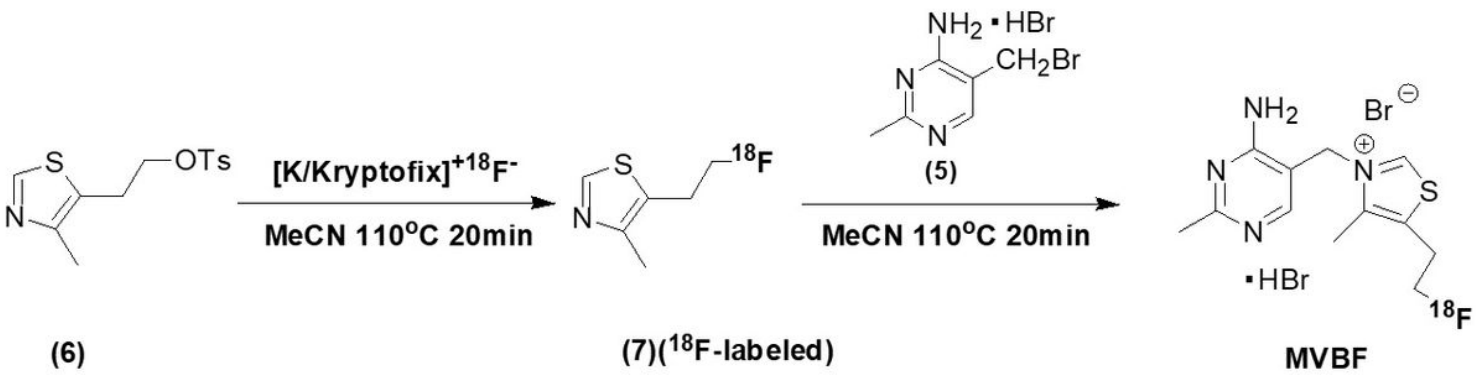

Figure 1

The Two-Step Synthesis of MVBF.

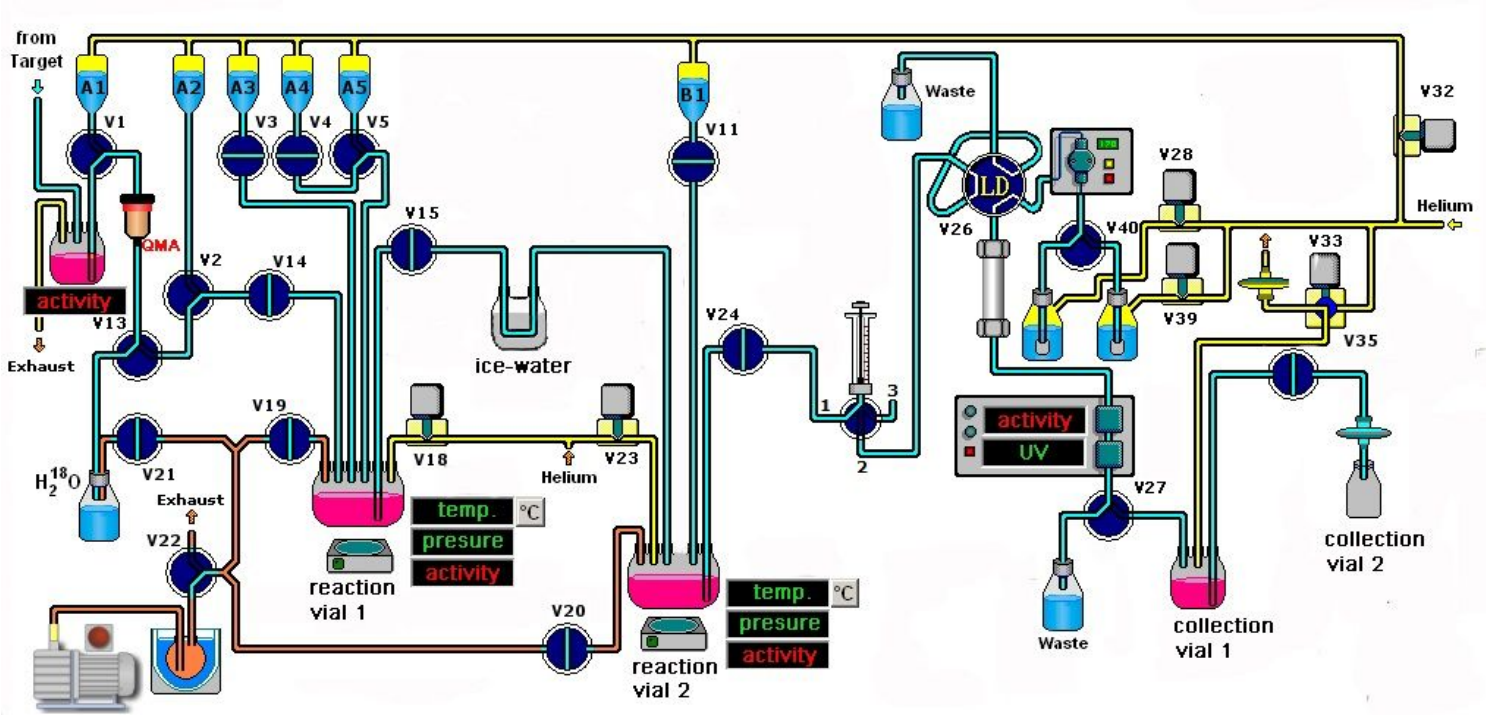

Figure 2

The Scheme of Automated Synthesis.

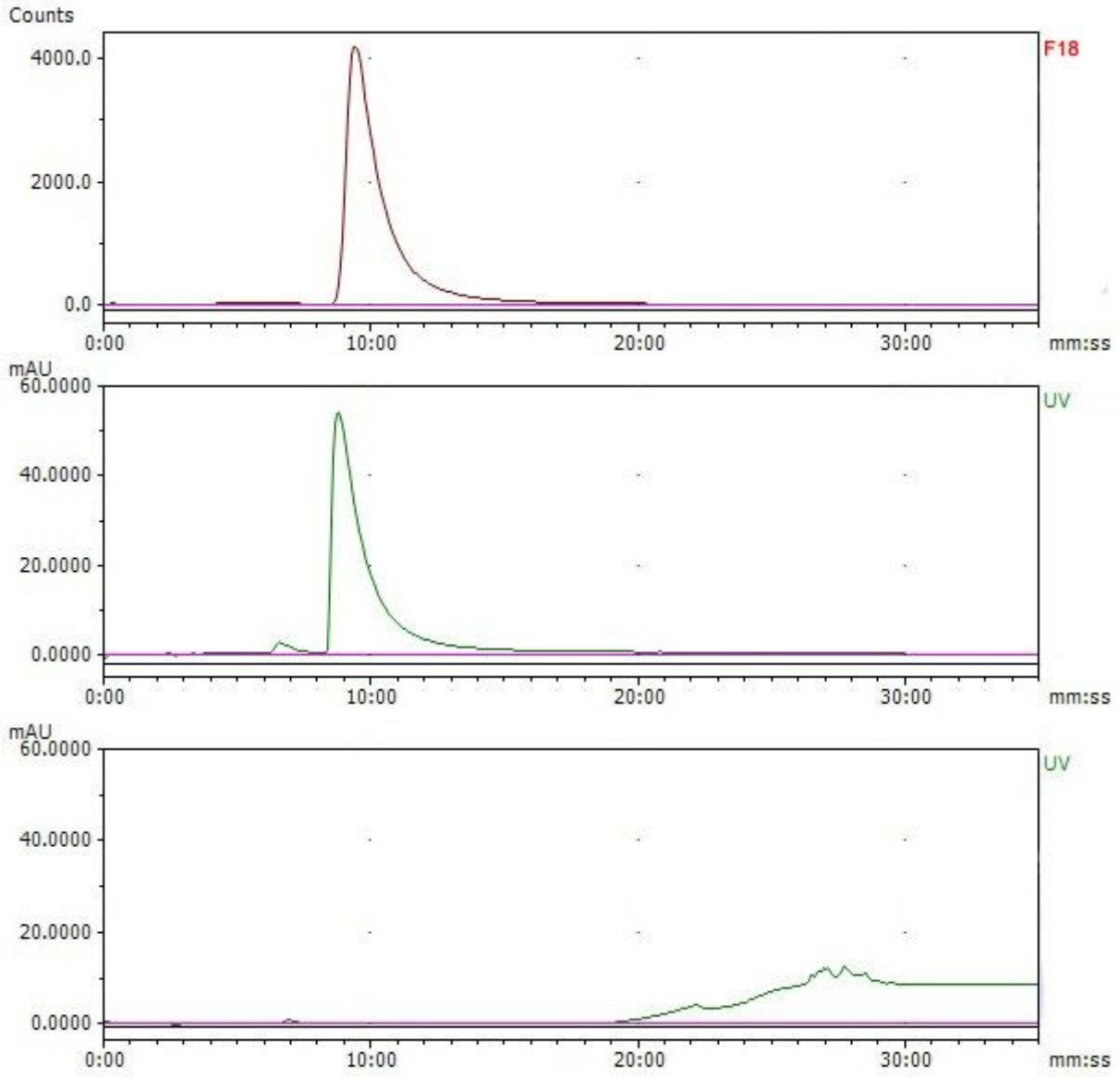

Figure 3

The Identity of MVBF and The Measurements of Radioactivity Purity and Specific Activity. A and B: results of coinjection of MVBF with cold standard sample. A was the radio-signal, and the retention time was 9 mins 24 secs; B was the UV-signal, and the retention time was 8 mins 47 secs. Radio-signal acquisition system was installed behind UV-signal acquisition system, and the time-lag was about half-minute at the flow rate of 0.8ml/min. Note that the peak shapes of A and B were the same. C: the UV signal of MVBF. UV=254nm.

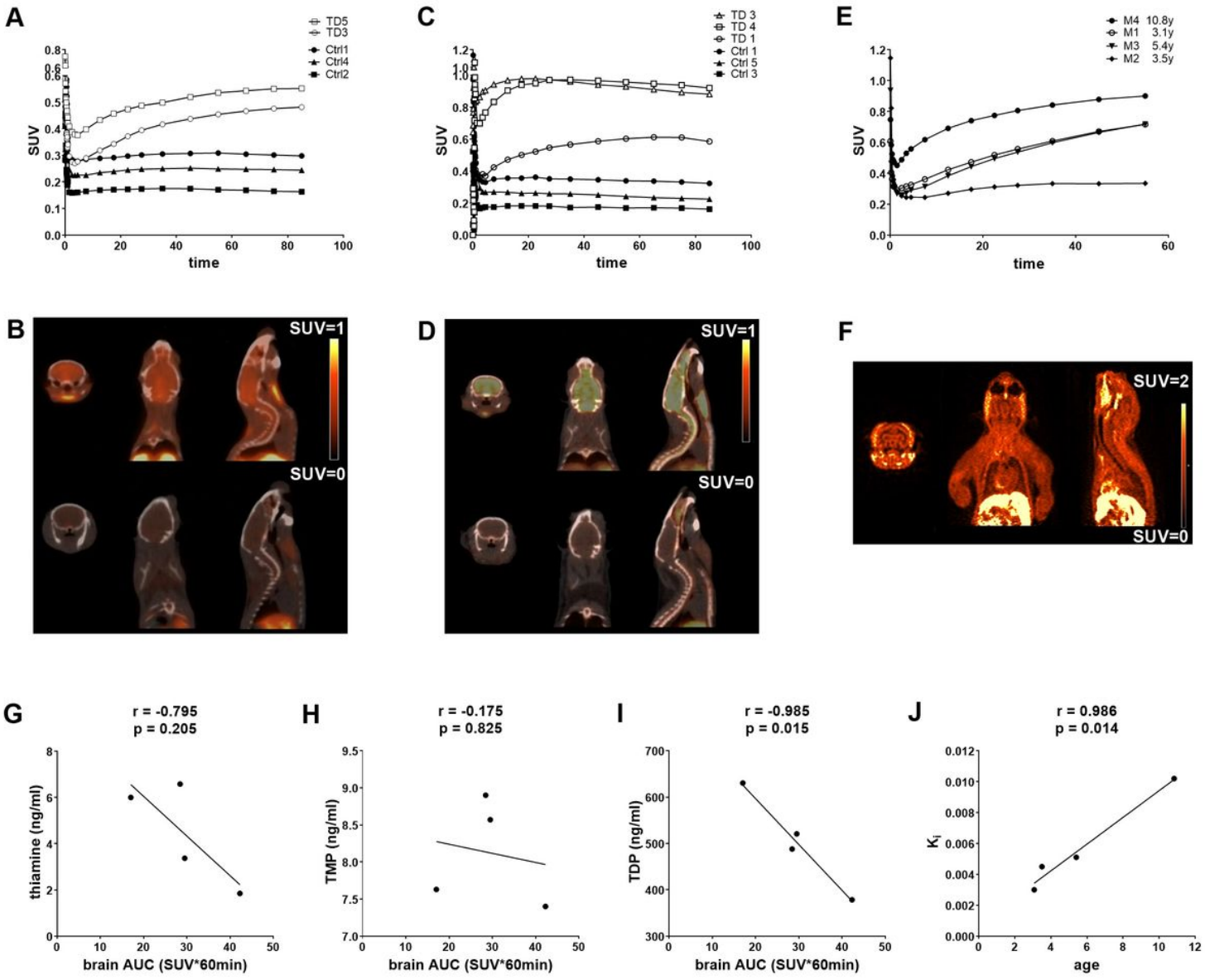

Figure 4

The Evaluation of Cerebral Thiamine Metabolism Status in Mice and Marmosets. A-B: C57 mice.A: the cerebral TACs of MVBF in 90 mins. The mean AUC value in two mice with TD was 1.9 times higher than that in control mice (38.73±3.74 vs. 20.38±3.23). B: The representative PET/CT images in TD and control groups (TD 5 and Ctrl 2, both at 50-60 min). C-D: ICR mice.C: the cerebral TACs of MVBF in 90 mins.The AUC values in mice with TD were significantly higher than those in controls (68.28±10.74vs. 21.88±4.25, P=0.016). D: The representative PET/CT images in TD and control mice (TD 4 and Ctrl 1, 50-60min). E-J: marmosets. E: the cerebral TACs of MVBF in 60 mins. F: the representative PET/CT images (M4, 30-60min). G, H, I: the correlations between cerebral AUC values of MVBF within 60 mins and blood levels of thiamine, TMP, and TDP. J: the correlation between cerebral transfer constant Ki and age.

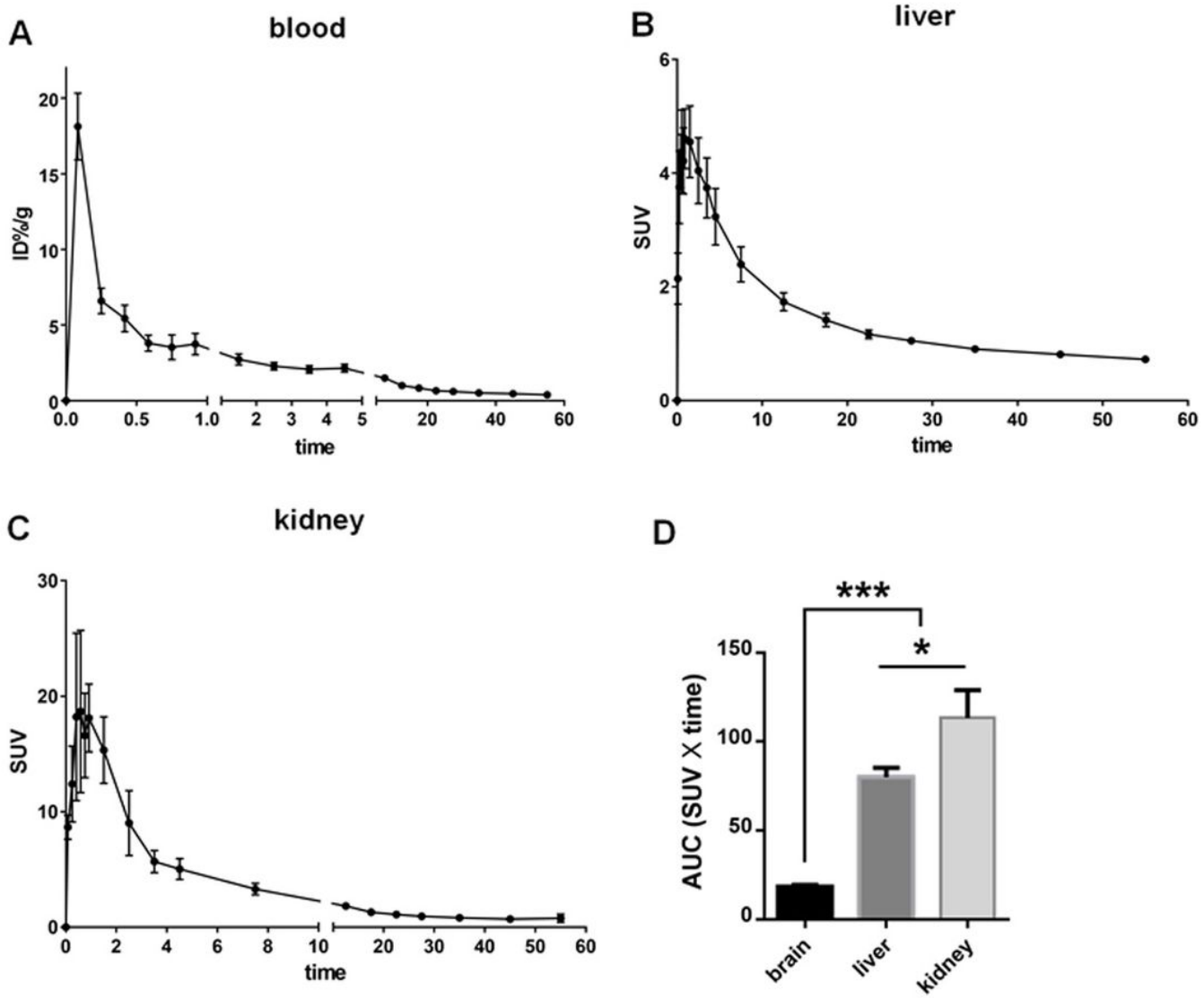

Figure 5

Studies of Pharmacokinetics and Metabolic Kinetics of MVBF in ICR Mice. A:The TAC of MVBF in blood (radioactivity expressed as ID%/g). B and C: the TACs of MVBF in liver and kidney, respectively (radioactivity expressed as SUV). D. Comparisons of AUC values within 60min between brain, liver and kidney. Note that the scale of X axes in A and C was changed properly. *, P<0.05. ***, P<0.001. repeated measurement of ANOVA with Trukey's post-hoc, n=5 for each graph.

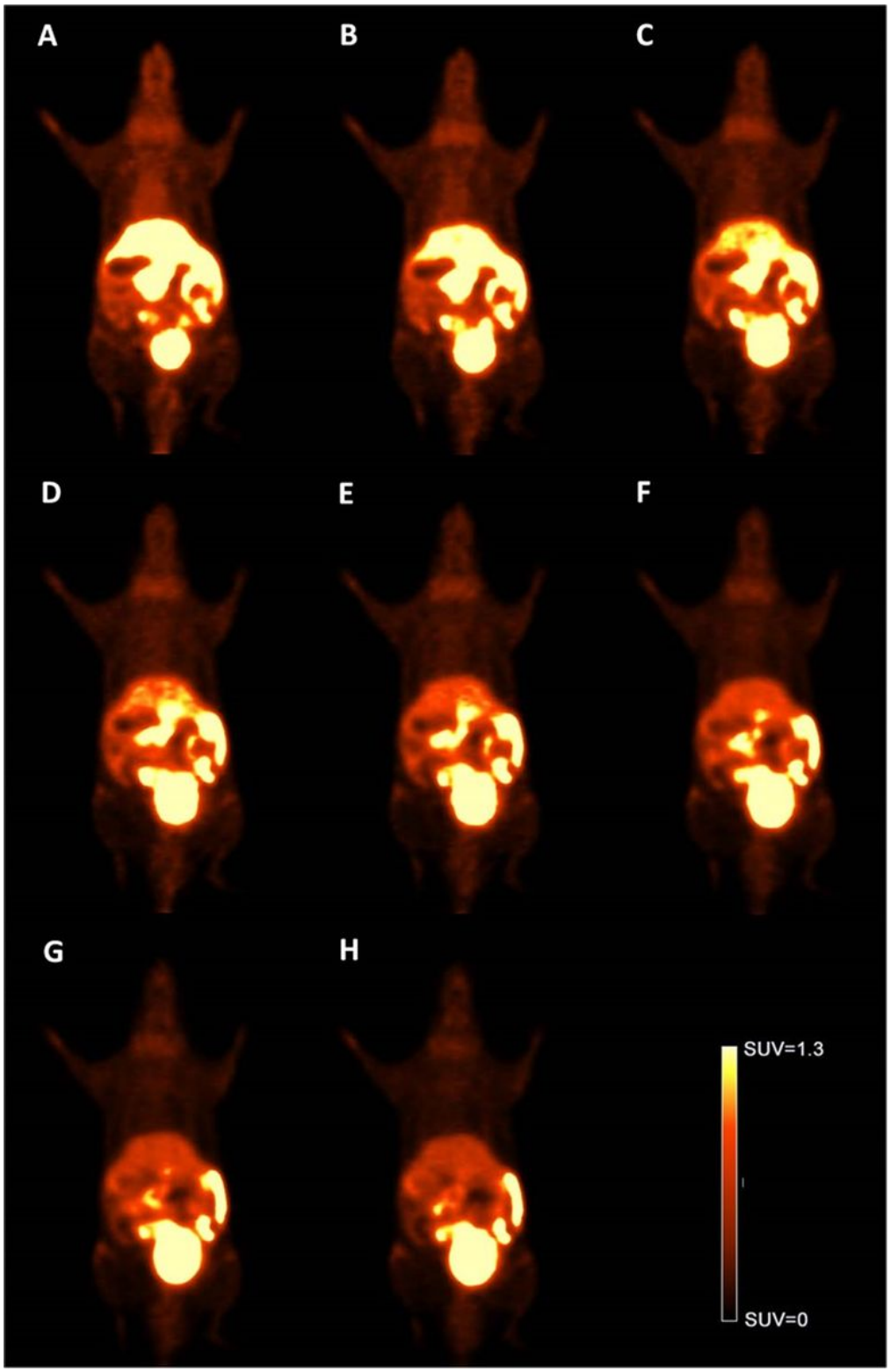

Figure 6

Dynamic Micro-PET/CT Scanning within 60 Mins The representative results from one ICR mouse. A. the 11th frame (5-10min). B. the 12th frame (10-15min). C. the 13th frame (15-20min). D. the 14th frame (20-25min). E. the 15th frame (25-30min). F. the 16th frame (30-40min). G. the 17th frame (40-50min). H. the 18th frame (50-60min).

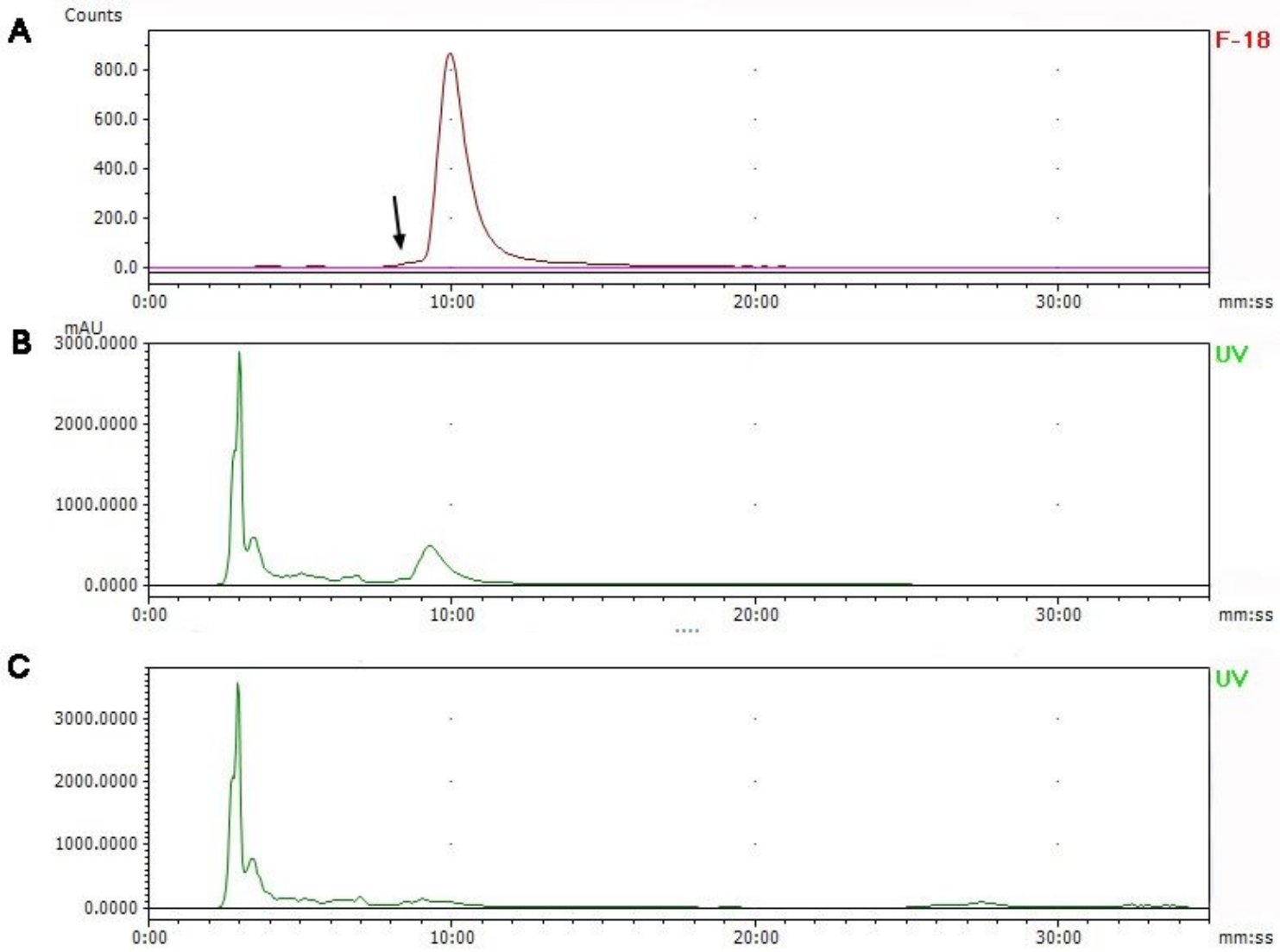

Figure 7

The Representative results of In Vivo Stability Study on MVBF. A and B: results for the mixture of mouse urine and cold standard sample of MVBF. A: the radio-signal, and the retention time of MVBF was 9 mins 54 secs. Note that the unknown metabolite(s) was ahead of MVBF (black arrow). B: the UV-signal, and the retention time of cold standard sample was 9 mins 14 secs. The UV-signal acquisition system was ahead of radio-signal and the time-lag was about half-minute. C: The UV signal of mouse urine. UV=254nm.

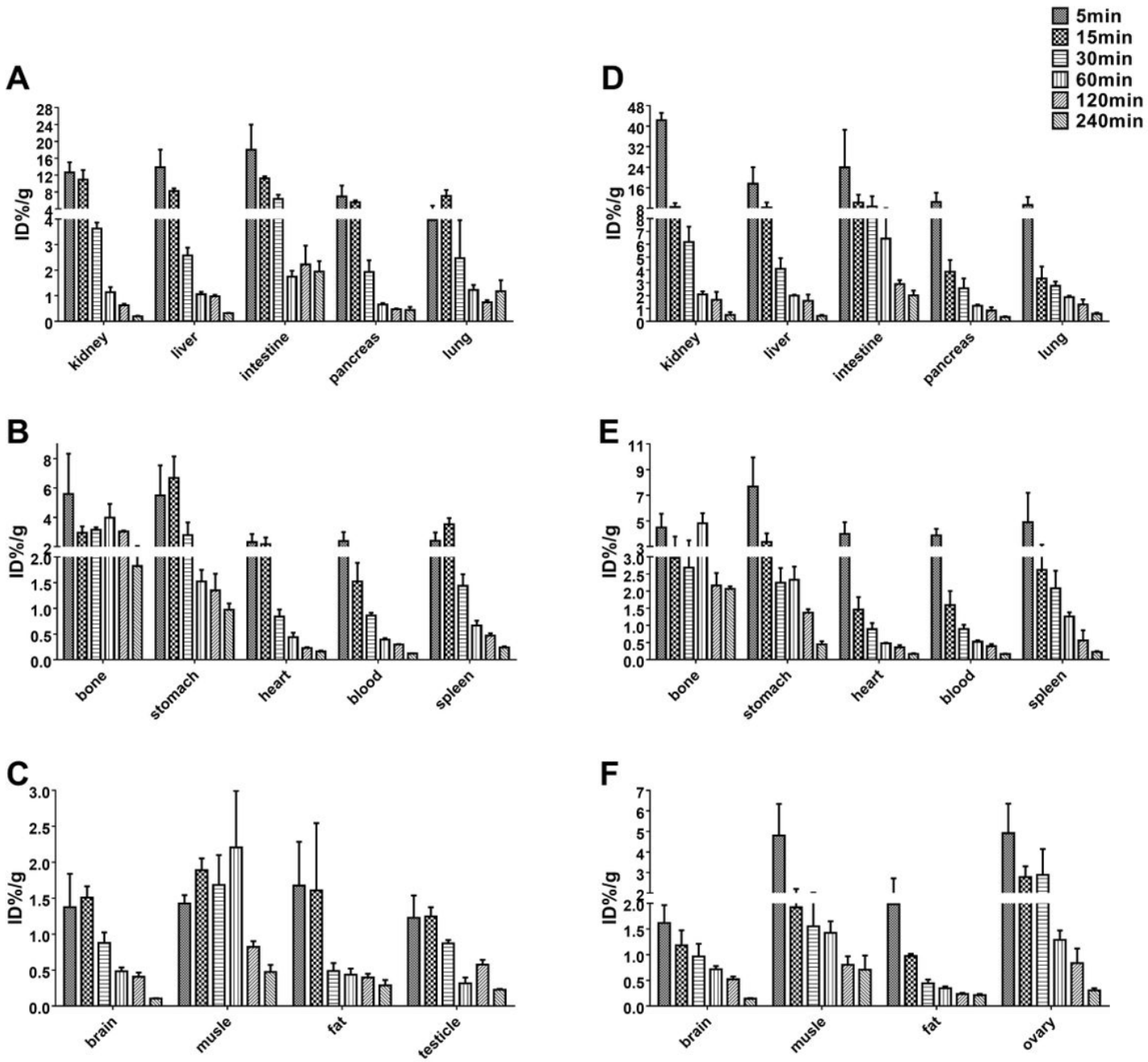

Figure 8

Biodistribution of MVBF in ICR Mice A-C: male. D-F: female. Radioactivity accumulation was expressed as %ID/g at 5, 15, 30, 60, 120, 240 min after tail-vein injection of 3.7 MBq MVBF in 0.1ml volume. n=3 for each organ or tissue at eact time point, cxcept for kidney, lung at 5min of male, and kidney, liver, duodenum, lung, ovary at 5min of female (n=2).

Supplementary Files

This is a list of supplementary files associated with this preprint. Click to download.

- SuppFig2.tif
- SuppFig1.tif
- SuppFig5.tif
- SuppFig6.tif
- SuppFig3.tif
- supplementarytext.docx
- SuppFig4.tif